Available online at www.sciencedirect.com

ScienceDirect

Procedia Engineering 10 (2011) 1081–1086

Engineering Procedia

ICM11

FE analysis of a notched bar under thermomechanical fatigue using a unified viscoplasticity model

D.W.J. Tanner*, W. Sun, T.H. Hyde

Materials, Mechanics and Structures Research Division, Faculty of Engineering
The University of Nottingham, Nottingham NG7 2RD, UK

Abstract

Z-mat software is used to implement the multiaxial form of the Chaboche unified viscoplastic constitutive equations into the Abaqus finite element (FE) code. Complex transient stress fields within a grade P91 steel notched bar specimen are investigated in detail for different thermomechanical fatigue (TMF) loading conditions. The results of this work can be used to determine suitable test conditions for notched specimens by providing predictions of the stress-strain history local to the notch. In future, such tests will be used along with the FE analyses to develop and validate multiaxial TMF lifing models.

Keywords: notched specimen; multiaxial TMF; Chaboche unified viscoplasticity; creep; finite element analysis

1. Introduction

The combination of cyclic (due to startup/shutdown and fluctuating operational demands) thermally and mechanically induced stresses can result in thermomechanical fatigue (TMF) failures in aero engine and power plant components (for example). Notches arising from geometrical discontinuities are sometimes referred to as 'hot spots' since they act as stress raisers and hence are locations where cracking and subsequent failure may initiate. For accurate fatigue life predictions to be made, the complex multi-dimensional stress-strain state at the root of a notch must be determined. Common analytical approaches based on stress concentration factors or strain energy density may be used for this purpose, but the finite element (FE) numerical method is a proficient alternative [1]. Realistic FE analyses rely on the

* Corresponding author. Tel.: +44 115 951 3811.
E-mail address: david.tanner@nottingham.ac.uk.

 doi:10.1016/j.proeng.2011.04.178

representative ability of the material behavior model used. Unified viscoplastic constitutive models have been successfully applied to describe the macroscopic behavior of materials where both rate-independent and rate-dependent effects occur simultaneously, e.g. during high temperature cyclic loading [2]. One of the most well known physical-phenomelogical models using state variables, developed in the framework of the thermodynamics of irreversible processes, was formulated by JL Chaboche. The Chaboche model [3] is appropriate for thermomechanical loading since it includes combined nonlinear isotropic and kinematic hardening, with a viscoplastic flow rule for time-dependent effects, including creep.

Once a suitable material model and the necessary material constants have been determined, attention can be focused on multiaxial fatigue life prediction methods, e.g. based on stress, strain or energy criteria [4]. Calibration and validation of such methods requires specimen tests under multiaxial loading. Since they introduce a three-dimensional (3D) stress state under uniaxial loading, notches can be machined into specimens in order to vastly simplify the testing procedure. Complex stress and strain fields evolve within a notched bar specimen experiencing TMF loading. FE modeling is an extremely useful tool for determining suitable loading parameters to induce a stress-strain state local to the notch that should give specimen failure in a reasonable number of cycles or time period.

The work in this paper makes use of Z-mat software (licensed by Transvalor/ENSMP) to implement the multiaxial form of the Chaboche constitutive equations into the Abaqus FE code. The complex transient stress fields within a grade P91 steel notched bar specimen are investigated in detail for four different representative TMF loading conditions.

2. Finite element model setup

2.1. Specimen geometry, loading and boundary conditions

Half of a cylindrical specimen with the geometry shown in Fig 1. was modeled using axisymmetry. A semi-circular notch of 2mm radius was centered at the midpoint of the whole specimen length. The FE mesh, refined around the notch, is also depicted in Fig 1., along with the symmetry boundary conditions indicated by the dotted lines, and arrows showing the end of the specimen used for mechanical loading, via either a displacement or stress cycle. The mesh contained 217, 8-node biquadratic axisymmetric quadrilateral elements with reduced integration points and 738 nodes. The temperature of the whole model was specified uniformly, and was either constant or cyclic, in the range of 400-600°C.

2.2. Material model

The Chaboche unified viscoplasticity model was used as presented in [2], where the total strain rate consists of the standard elastic and thermal components, in addition to the viscoplastic strain rate, $\dot{\varepsilon}_p$, given by the following equation, in uniaxial form:

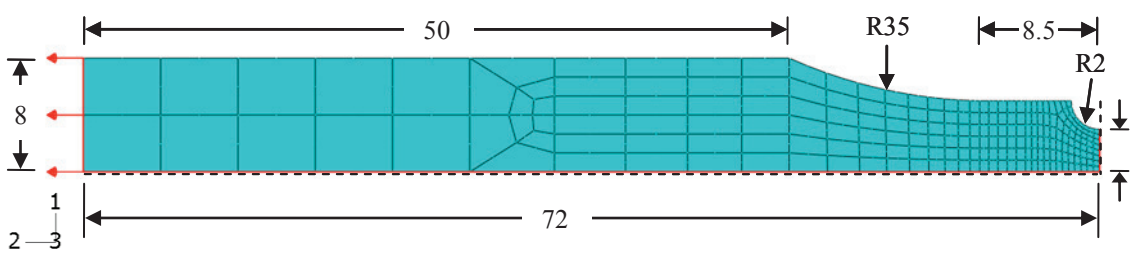

Fig. 1. Model geometry with FE mesh, and loading and boundary conditions (dimensions in mm)

$$\dot{\varepsilon}_p = \left\langle \frac{f}{Z} \right\rangle^n \mathrm{sgn}(\sigma - \chi)$$

where

$$\mathrm{sgn}(x) = \begin{cases} 1, & x > 0 \\ 0, & x = 0 \\ -1, & x < 0 \end{cases} \quad , \quad \langle x \rangle = \begin{cases} x, & x > 0 \\ 0, & x \le 0 \end{cases}$$

and

$$f = |\sigma - \chi| - R - k$$

Z and n are material constants, σ is the applied stress, k is the initial cyclic yield stress, χ is a kinematic hardening parameter and R is an isotropic hardening parameter given by:

$$\begin{aligned} \chi &= \chi_1 + \chi_2 \\ \dot{\chi}_i &= C_i(a_i \dot{\varepsilon}_p - \chi_i \dot{p}) \\ R &= Q(1 - e^{-bp}) \\ \sigma_v &= Z\dot{p}^{1/n} \\ \dot{p} &= |\dot{\varepsilon}_p| \end{aligned}$$

where σ_v is the viscous stress; p is the accumulated viscoplastic strain; a_i and C_i (i=1,2) represent the stationary values of χ_i and the speed to reach the stationary values, respectively; Q is the asymptotic value of the isotropic variable, R, at the stabilized cyclic condition and b governs the stabilization rate. The applied stress can be decomposed as:

$$\sigma = \chi + (R + k + \sigma_v)\,\mathrm{sgn}(\sigma - \chi)$$

The required temperature dependent material constants for the martensitic steel P91 were also taken from [2] and are reproduced in Table 1. Temperature independent values of Poisson's ratio and thermal strain coefficient were specified as 0.3 and 14.5×10^{-6}/°C, respectively.

Table 1. Material constants for P91 (from [2])

Temp. (°C)	E (MPa)	k (MPa)	Q (MPa)	b	a_1 (MPa)	C_1	a_2 (MPa)	C_2	Z (MPa $s^{1/n}$)	n
400	187537.0	96	-55.0	0.45	150.0	2350.0	120.0	405.0	2000	2.25
500	181321.6	90	-60.0	0.6	98.5	2191.6	104.7	460.7	1875	2.55
600	139395.2	85	-75.4	1.0	52.0	2055.0	67.3	463.0	1750	2.7

3. Results

The results from four different load cases are presented in Figs 2-5. Figs 2(a), 3(a), 4(a) and 5(a) show the stress (σ_{22}) or displacement (U2) cycle applied to the loading end of the model (see Fig. 1), and the temperature history specified throughout the model. The evolution of von Mises equivalent stress (σ_{eq}) and axial stress (σ_{22}) at nodal points at different radial distances (R) across the plane of the minimum section measured from the centerline, are plotted in Figs 2(b), 3(b), 4(b) and 5(b), and Figs 2(c), 3(c), 4(c) and 5(c), respectively.

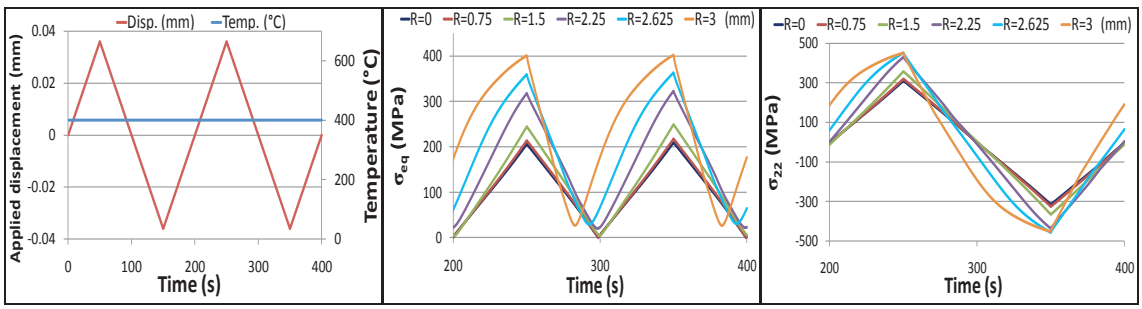

Fig. 2. Results for 400°C displacement control (a) loading; (b) von Mises equivalent stress; (c) axial stress

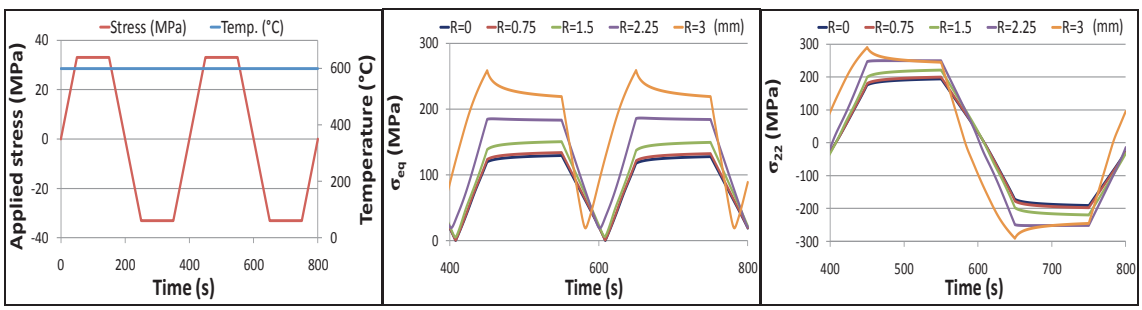

Fig. 3. Results for 600°C stress control with hold periods (a) loading; (b) von Mises equivalent stress; (c) axial stress

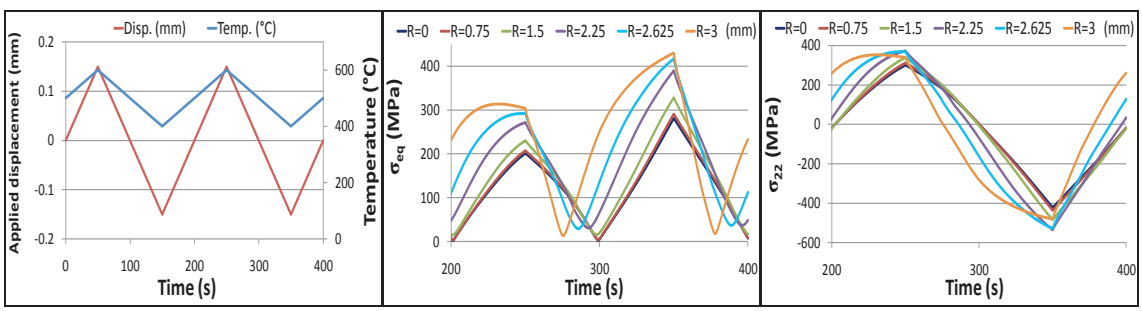

Fig. 4. Results for 400-600°C IP displacement control (a) loading; (b) von Mises equivalent stress; (c) axial stress

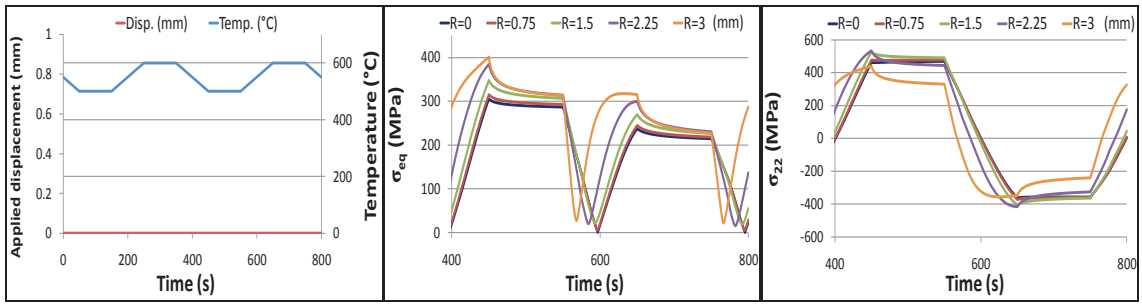

Fig. 5. Results for 500-600°C with hold periods and zero displacement (a) loading; (b) von Mises equivalent stress; (c) axial stress

Results from a 400°C isothermal, displacement control case are shown in Fig 2. The von Mises equivalent stress increases significantly with the radial distance from the centre of the specimen to the outside surface, and therefore it peaks at the notch root as this is the point where the multiaxial stress induced by the geometry of the notch is greatest. Plastic yielding is evident at the points towards the outside of the specimen. It is interesting to note that the peak axial stress actually occurs a small distance inside the specimen away from the notch root. The axial stress at the root of the notch is limited by the greater yielding that it undergoes.

Fig 3. depicts a 600°C isothermal, stress control case with hold periods at maximum tensile and compressive load. Stress redistribution across the plane of the minimum section is evident due to creep during the hold periods. The high stress at the root of the notch decreases whilst the stresses on the specimen inside increase to maintain equilibrium. There is a point, R=2.25mm where the stress is constant during the hold periods. The axial stress here is actually higher in magnitude at the end of the hold periods than that at R=3mm, the root of the notch.

Results from a 400-600°C displacement control case where the mechanical and thermal loading were in-phase (IP) are presented in Fig 4. By examining the equivalent stress at the notch root it is clear that the increase in temperature to the peak at 250s has given the expected reduction in the material's yield stress. The greater extent of plastic yielding has caused the position of the peak axial stress to move further inside the specimen compared with the 400°C isothermal, displacement control case presented in Fig 2.

Figs 5 and 6 contain results for a constrained displacement case with a 500-600°C thermal cycle with hold periods at maximum and minimum temperature. Stress relaxation due to creep occurs during the hold periods. The effect of reduction in yield stress with increasing temperature is also noticeable. High stresses are evident in this case, which shows how severe the effects of thermal loading can be when displacement is constrained. The greater yielding and stress relaxation at the notch root has actually caused the peak tensile and compressive axial stresses to be at a minimum here.

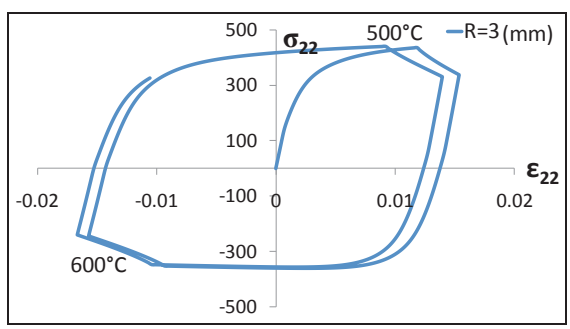

Fig. 6. Axial stress-strain loops at notch root for 500-600°C case with hold periods and constrained displacement

4. Discussion and conclusions

Z-mat software was used to implement the multiaxial form of the Chaboche unified viscoplastic constitutive equations into the Abaqus FE code. Complex transient stress fields within a grade P91 steel notched bar specimen were investigated in detail for four different representative TMF loading conditions. The material data and methodology used has been shown to give results that correlate well with displacement measurements made over a gauge length that included a notch during laboratory testing [5].

Mechanical stress/displacement and iso/cyclic thermal behavior was studied. Two of the cases also contained hold periods during the cycles to allow for noticeable creep to occur. Stress relaxation and redistribution around the notch due to creep was predicted. The model was shown to be capable of computing complex multiaxial stress-strain behavior e.g. for a constrained displacement, cyclic thermal case, that generated out-of-phase (OP) mechanical and thermal loading (Figs 5 and 6), which practically could not be produced without the use of FE analysis. The data presented was taken from the first few load cycles to limit the computation time but the trends would be expected to remain the same, although the magnitudes of the stresses may change in later cycles due to material hardening/softening behavior.

The results of this work can be used to determine suitable test conditions for notched specimens by providing predictions of the stress-strain history local to the notch. In future, such tests will be used along with the FE analyses to develop and validate multiaxial TMF lifing models.

Acknowledgements

The authors would like to acknowledge the support of The Energy Programme, which is a Research Councils UK cross council initiative led by EPSRC and contributed to by ESRC, NERC, BBSRC and STFC, and specifically the Supergen initiative (Grants GR/S86334/01 and EP/F029748) and the following companies; Alstom Power Ltd., Doosan Babcock, E.ON, National Physical Laboratory, Praxair Surface Technologies Ltd, QinetiQ, Rolls-Royce plc, RWE npower, Siemens Industrial Turbomachinery Ltd. and Tata Steel, for their valuable contributions to the project.

References

[1] Hurley PJ, Whittaker MT, Williams SJ, Evans WJ. Prediction of fatigue initiation lives in notched Ti 6246 specimens. *Int J Fatigue* 2008;**30**(4):623–634.

[2] Saad AA, Hyde CJ, Sun W, Hyde TH. Thermal-mechanical fatigue simulation of a P91 steel in a temperature range of 400-600°C. In: *Proc. HIDA-5*, Guildford, UK; 2010 [CD-ROM].

[3] Chaboche JL, Rousselier G. On the plastic and viscoplastic constitutive equations---Part I: Rules developed with internal variable concept. *J Press Vess-T ASME* 1983;**105**(2):153–8.

[4] Karolczuk A, Macha E. A review of critical plane orientations in multiaxial fatigue failure criteria of metallic materials. *Int J Fracture* 2005;**134**(3):267–304.

[5] Saad AA, Hyde TH, Sun W, Hyde CJ. Constitutive model development of P91 steel and its simulation in TMF conditions. Submitted to *ESIA11*, Manchester, UK; May 2011.